



This is a repository copy of *Towards understanding the surface friction in rotational-vibration assisted incremental sheet forming*.

White Rose Research Online URL for this paper:

<https://eprints.whiterose.ac.uk/220834/>

Version: Published Version

Article:

Chang, Z., Peng, W. and Long, H. orcid.org/0000-0003-1673-1193 (2025) Towards understanding the surface friction in rotational-vibration assisted incremental sheet forming. *Journal of Materials Processing Technology*, 336. 118692. ISSN 0924-0136

<https://doi.org/10.1016/j.jmatprotec.2024.118692>

Reuse

This article is distributed under the terms of the Creative Commons Attribution (CC BY) licence. This licence allows you to distribute, remix, tweak, and build upon the work, even commercially, as long as you credit the authors for the original work. More information and the full terms of the licence here:

<https://creativecommons.org/licenses/>

Takedown

If you consider content in White Rose Research Online to be in breach of UK law, please notify us by emailing eprints@whiterose.ac.uk including the URL of the record and the reason for the withdrawal request.



eprints@whiterose.ac.uk
<https://eprints.whiterose.ac.uk/>



Research article

Towards understanding the surface friction in rotational-vibration assisted incremental sheet forming

Zhidong Chang, Wenxuan Peng, Hui Long*

Department of Mechanical Engineering, the University of Sheffield, Sir Frederick Mappin Building, Sheffield S1 3JD, UK

ARTICLE INFO

Keywords:

Incremental sheet forming
 Surface quality
 High-amplitude vibration
 Coefficient of friction
 Analytical modelling

ABSTRACT

Incremental sheet forming (ISF), as a flexible sheet metal forming method, has attracted wide-spreading attention, however the dissatisfied surface quality has limited its adoption for potential industrial applications. There are insufficient studies in assessing the friction condition in ISF and it also lacks accurate methods for determining the coefficient of friction (CoF). Further investigations are required to understand fundamental mechanisms of the effect of friction condition on surface quality in ISF. In this study, it is found that the surface quality of sheet metal parts is considerably improved by rotational-vibration assisted ISF (RV-ISF) process under high-amplitude vibration. The improvement is considered to be attained by several underpinning mechanisms: the friction reduction under vibration, improvement of lubrication condition and increased surface micro-hardness. To investigate these mechanisms, two methods are proposed to evaluate the friction condition at the contact interface between the tool and sheet in ISF. The first method is a new calibration model for an accurate calculation of the CoF in ISF by excluding the effect of the horizontal forming force of the ISF tool. The second method is a novel analytical model in predicting the reduction of CoF under vibration in the RV-ISF. The friction prediction model is validated through experimental results when employing various rotational-vibration tools in processing three different materials. The results show that the forming procedure of “down-milling” is better than “up-milling” for improving the surface quality in RV-ISF. The vibration amplitude has the greatest effect on friction reduction, while other variables including non-vibrating frictional force, contact rigidity coefficient and tool radius also show significant effects on friction reduction. This study presents a significant advancement of friction research in ISF by developing two new friction models, offering new insights and effective methods to improve surface quality and accurately calculate the CoF under vibration effect.

1. Introduction

The increased demand for improved surface quality of the sheet metal products has prompted the development of novel forming processes that can overcome limitations associated with conventional forming technologies. The introduction of the vibration field during forming processes has emerged as a promising approach for surface quality improvement, especially in incremental sheet forming (ISF) processes, where surface quality and friction conditions are critical for enabling further industrial applications of this flexible sheet forming technology.

Vibration-assisted (VA) forming technology has been developed through introducing a controllable vibration field to the deforming material or forming tools or dies during the forming process. The fluctuated stresses caused by the vibration field in the vibration-assisted

forming (VAF) process has shown its beneficial effect on reducing material flow stress [1], improving friction condition [2] and optimising surface quality [3]. The mechanisms of a vibration field for surface quality improvement in the VAF process can be summarised into two effects: volume effect and surface effect. The volume effect refers to the dislocation movement and grain refinement within the sheet material, which results in improved material ductility and reduced forming forces. In contrast, the surface effect is primarily related to the reduction of interfacial friction and the enhancement of surface finish, as the vibration field promotes smoother material flow and obtains better lubrication conditions. Concerning on the surface effect in VAF, Xie et al. [4] demonstrated that the coefficient of friction for AA6063 sheets was significantly reduced by applying ultrasonic vibration during an upsetting experiment, and the reduction effect was closely related to the vibration amplitude, which was also observed by Yao et al. [5]. Bai et al. [6] attributed the surface effect to the promotion of material flow during

* Corresponding author.

E-mail addresses: 1079099007@sjtu.edu.cn (Z. Chang), wx.dusk.peng@gmail.com (W. Peng), h.long@sheffield.ac.uk (H. Long).<https://doi.org/10.1016/j.jmatprotec.2024.118692>

Received 11 November 2024; Received in revised form 6 December 2024; Accepted 6 December 2024

Available online 7 December 2024

0924-0136/© 2024 The Authors. Published by Elsevier B.V. This is an open access article under the CC BY license (<http://creativecommons.org/licenses/by/4.0/>).

Nomenclatures			
μ	Coefficient of friction at the contact interface between the tool and sheet	s	Elastic deformation of roughness asperities along the tool tangential direction
μ^*	Friction indicator	s_1	Elastic deformation of roughness asperities after time interval Δt
α	Wall angle of sheet part	y_p	Vibrating displacement of the tool along the radial direction
t_0	Initial sheet thickness	A	Vibrating amplitude of the sheet
R	Tool radius	v_d	Feed rate of the tool
h	Step size of the tool	ω	Rotational speed of the tool
h_s	Scallop height on the formed part	v_r	Relative velocity between the tool and sheet
h_1	Reduction of sheet thickness at the bottom of the contact area	F_c	Non-vibrating frictional force in conventional ISF
F_f	Frictional force of the tool	n	Number of time intervals in the entire vibration cycle
F_z	Axial force of the tool	θ	Rotational angle of the tool after time interval
k_t	Contact rigidity along the tool tangential direction	r	Ratio of frictional force reduction between conventional ISF and RV-ISF

the plastic deformation superimposed with ultrasonic vibrations. Pohlman and Lehfeldt [7] demonstrated that the friction reduction due to the surface effect had been achieved by the increase of the relative sliding speed during ultrasonic VAF, but it disappeared once the sliding speed exceeded a critical value. Wang et al. [8] investigated the friction reduction due to the surface effect for C45 steel sheets under vibrations applied in different directions, and found that the vibration exerted along the relative sliding direction showed the best effect on the reduction of friction. Wan et al. [9] investigated the characteristics of variations of the interfacial friction between the die cavity and surface of T2 copper sheets during ultrasonic-assisted micro-extrusion experiment, and found that the coefficient of friction and the extrusion force were decreased with the increasing of the ultrasonic amplitude. It is clear that the superposition of a vibration field onto the surface of a material during the forming process has significant advantages in reducing the interfacial friction for most metals, which is extremely important to improve surface quality of formed products for industrial applications.

Different from the ultrasonic vibration, the low-frequency vibration exhibits its unique advantages in VAF process. Hung and Tsai [10] observed that the vibration softening effect decreased significantly with the increasing of the sample size for Brass C2600 material during ultrasonic-assisted upsetting, due to the decrease of the absorbed energy from ultrasonic vibration per unit volume of the sample material. This phenomenon inspired studies to introduce the low-frequency vibration with large excited forces into the sheet metal during VAF process. Ali et al. [11] demonstrated that exerting a vibrated blank holder force at 0–10 Hz in a deep drawing process produced high-quality products of DC04 and AA5754 materials without any sheet tearing or wrinkles. Meng et al. [12] exerted a low-frequency vibration field along the normal direction to the specimen during uniaxial tensile test of DC04 steel and found that the tensile force under superimposed vibration was reduced by 23.7 % compared with that without the vibration field. Lin et al. [13] found that the assisted vibration field with low-frequency accelerated the dislocation migration and crystal torsion of Ti45Nb wire material, promoting the dislocation annihilation among the shearing band of the material. The friction reduction phenomenon could be also found under the low-frequency VAF forming processes. Maeno et al. [14] and Behrens et al. [15] observed the decrease of the forming force and the improvement of surface quality during the VA compression process with low-frequency vibration. Matsumoto et al. [16] attributed the improvement of the surface quality to the auto-fill of the lubrication oil resulting from the elastic deformation between the AA6061-T6 sheet and the die under the vibration field. Zhang et al. [17] considered that the surface quality was improved due to the decrease of friction and material accumulation with a low-vibration frequency.

In conclusion, the decrease of the forming force and optimisation of surface quality have also been observed in VAF processes under low-

frequency vibration fields, similar to that under the high-frequency ultrasonic vibration field. However, the adoption of the ultrasonic vibration in VAF shows limited effects on improving surface quality and reducing material flow stress due to its low-amplitude and vibration energy, making VAF with the ultrasonic vibration inapplicable to large-sized components. Compared with the ultrasonic vibration field, the low-frequency vibration field is characterised by high-amplitude and high excitation force, so that higher vibration energy can be applied to the deforming material to further improve the surface quality and formability of different materials. Therefore, the investigation on the surface effect on the friction behaviour under the low-frequency vibration field is important for the application of VAF for large-sized components using various materials.

As a flexible sheet metal forming process, incremental sheet forming (ISF) is especially applicable for small-batch manufacturing of sheet metal products with free-form geometries. To better understand its deformation mechanisms, numerous analytical models have been developed in recent years. For instance, Filice et al. [18] studied the stress state and deformation mode of the deforming sheet metal, highlighting significant hydrostatic pressure in the deformation zone. Durante et al. [19] proposed a model to assess surface roughness based on the forming angle of the formed part, and step size and tool diameter. Hamilton et al. [20] examined the effects of tool feed rate and spindle rotational speed on surface roughness and developed a model for predicting orange peel damage on the formed surface, offering guidelines to enhance surface quality. Moreover, research into the friction behaviour in single-point incremental forming (SPIF) process has received considerable attention. Park et al. [21] introduced friction stir incremental sheet forming (FSISF), which utilising the heat generated by high friction between the rotating tool and the unlubricated sheet to significantly enhance the formability of magnesium alloys, offering a new approach for expanding the applications of ISF technology.

To extend the ISF process to form some low-ductility sheet materials, the vibration-assisted ISF (VAISF) process has been proposed by introducing a vibration field into sheet metal during the ISF process. Cheng et al. [22] introduced the ultrasonic vibration into ISF process, demonstrating its effective advantages in decreasing the forming force and improving the formability of AA1050. Long et al. [23] and Bai et al. [24] observed a significant reduction in forming forces for materials with higher yield strength, through increasing vibration energy and reducing tool feed rate. Amini et al. [25] highlighted the positive impact of the ultrasonic vibration on sheet metal formability, and noted an enhancement in the hardness of surface material under VAISF process. Li et al. [26] established a constitutive model for describing the constitutive behaviour of sheet materials under ultrasonic vibration. Different from the high-frequency vibration ISF processes, Lu et al. [27] applied low-frequency vibrations with high-amplitude in SPIF using offset tools,

generating conical parts with ultrafine grain structures in magnesium alloy AZ31B. Long et al. [28] proposed a novel rosette tool design concept by cutting small grooves on the tool surface in developing rotational vibration-assisted incremental sheet forming (RV-ISF) process, creating vibrations with low-frequency and high-amplitude for formability improvement of magnesium alloy AZ31B. As demonstrated by the above studies, the formability of sheet materials in VAISF processes have been systematically investigated, while the influence of the vibration field on the friction condition and surface quality has not been investigated.

To overcome the issue of dissatisfied surface quality of ISF, several methods have been proposed and investigated, such as optimising process parameters or application of a vibration field in ISF. However, research gaps still remain to understand the effect of vibration field with low-frequency and high-amplitude on surface quality in ISF, and to investigate fundamental mechanisms of vibration field on improving friction condition and surface quality. In addition, numerous research

has been conducted concerning the influences of different forming conditions on the surface quality in ISF, but an accurate description of friction condition in ISF has not been found. The traditional Coulomb's friction model is not applicable to determine the coefficient of friction in ISF because the spherical crown shape of the tool contact surface makes the horizontal force not equal to the frictional force. Therefore, understanding the effect of low-frequency and high-amplitude vibration field on ISF friction condition and developing accurate models for determining the CoF in ISF are extremely important for the improvement of surface quality in ISF.

In this study, a series of experiments as well as analytical modelling together with microstructure characterisation have been conducted to investigate the mechanisms of the improved surface quality during the RV-ISF and the influences of rotational-vibration tools on the surface quality. A new calibration model of calculating the CoF has been developed by excluding the horizontal forming force from the calculation of frictional force to better analyse the effect of friction in ISF.

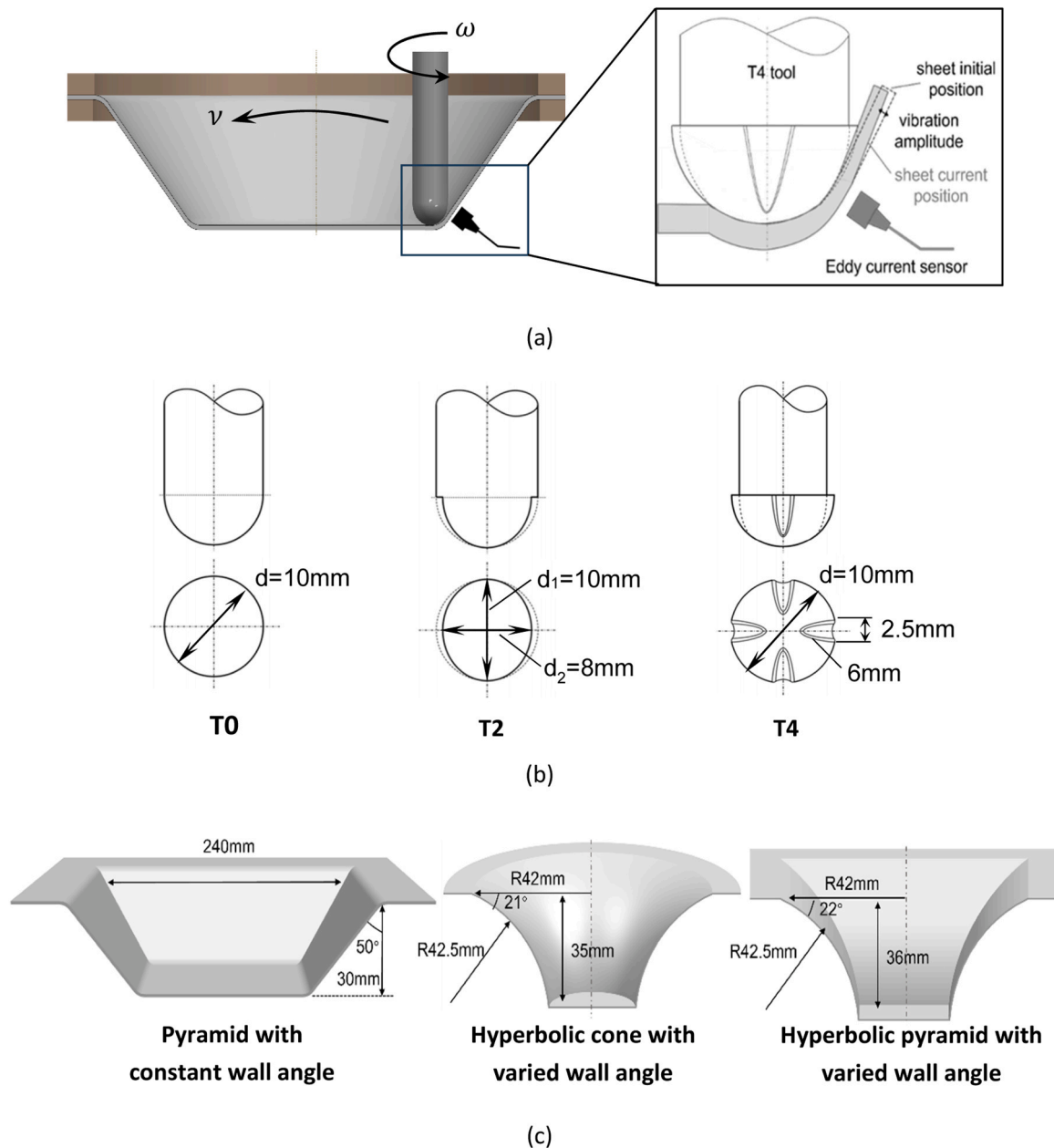


Fig. 1. Experimental design of rotational vibration-assisted incremental sheet forming (RV-ISF). (a) Schematic of RV-ISF experiment and vibration measurement by Eddy current sensor. (b) Conventional tool T0 and rotational-vibration tools T2 and T4. (c) Formed geometries.

Furthermore, a new analytical model has been proposed in this study to assess the impact of the vibration field on surface friction, validated through a series of experiments. This study addresses a key research gap of understanding friction behaviour and fundamental mechanisms by investigating the effect of low-frequency and high-amplitude vibration and developing two new friction models, providing effective methods to improve surface quality under vibration effect in ISF.

2. Methods

2.1. Experiment of rotational vibration-assisted ISF (RV-ISF)

To overcome the limitations of ultrasonic vibration in forming low ductility materials and large sized parts, the Rotational Vibration-assisted Incremental Sheet Forming (RV-ISF) process [28] is investigated in this study by using a specific shaped tool to exert a vibration field with low-frequency and high-amplitude onto sheet metal, as illustrated in Fig. 1a. In contrast to the conventional spherical tool (T0), the rotational-vibration T2 tool has an ellipsoidal end creating two offsets while the T4 tool is designed with four-grooves, as shown in Fig. 1b. The design rationale of the rotational-vibration tools is that offsets or grooves on the tool surface create intermittent contacts between the sheet metal and the tool as the tool rotates, resulting in the localised vibration of the sheet when the tool loses the contact with the sheet at offset and groove location [28]. Through the rotation of the specifically designed tool, localised vibration fields can be created to the sheet metal with lower frequency and higher amplitude than that by the ultrasonic vibration field. Fig. 1c shows the geometries of the RV-ISF parts used to investigate the influence of rotational vibration on surface friction of the sheet in this study. In order to measure the vibration frequency and amplitude generated by the different tools in the RV-ISF process, an Eddy current sensor is used to detect the vibration of the sheet, as illustrated in Fig. 1a.

A series of experiments by using different tools (T0, T2 and T4) and different materials (AA5251, AA6082, and AZ31B) are conducted. The variable-angle hyperbolic cone parts are produced by using AA5251 and AA6082 sheet materials, and the variable-angle hyperbolic pyramid parts are produced by using AZ31B sheet material. The process parameters and material parameters used in the experiments are listed in Table 1.

2.2. New calibration model for calculating coefficient of friction in ISF

The concept of friction indicator, extensively employed in sheet metal forming research, was proposed by Xu et al. [29], defined as the ratio of the horizontal and vertical forming forces. However, as illustrated in Fig. 2a,b, it overestimates the actual friction effect in the ISF process, because the horizontal forming force is included in the calculation of the friction indicator. This results in the value of the friction indicator being much higher than the actual CoF. The friction indicator can only be used for qualitative analysis thus limiting its application to improve surface quality in ISF. An accurate model for calculating the CoF is required to investigate the effect of surface friction on surface quality in an ISF process using different tools.

To achieve a more accurate calculation of the CoF for evaluating the friction condition in ISF process, a new calibration model of the CoF is

Table 1
Material and process parameters used in the validation models.

Materials	t_0 (mm)	h (mm)	R (mm)	ω (RPM)	ν (mm/ min)	k_t (N/ μm)	F_c (N)
AA5251	0.9	0.3	5	7000	1000	67.3	180
AA6082	1	0.3	5	3000	1000	67.3	240
AZ31B	1	0.3	5	4000	1000	48	62

proposed in this study by excluding the horizontal forming force from the calculation of the frictional force in ISF. It is difficult to calculate the horizontal forming force directly, however the effect of the horizontal forming force components on the CoF can be characterised indirectly using the contact area between the tool and deforming sheet.

Based on the definition of the friction indicator shown in Eq. (1), the effect of horizontal forming force components can be expressed in terms of the contact area:

$$\mu^* = \frac{F_{forming} + F_{friction}}{F_z} = \frac{F_{friction}}{F_z} + \frac{S_h \sigma_t}{S_z \sigma_t} = \mu + \frac{\sqrt{S_r^2 + S_t^2}}{S_z} \quad (1)$$

where $F_{forming}$, $F_{friction}$, F_z and σ_t are the horizontal forming force, frictional force, vertical forming force, and through-thickness stress, respectively. As shown in Fig. 2c, the decomposed contact areas perpendicular to the axial, tangential, and radial directions of the deforming sheet are defined as S_z , S_t and S_r , respectively, which can be obtained from Chang et al. [30]:

$$\begin{cases} S_z = \frac{\pi}{4} [R^2 - (R - h_1)^2] \left(1 + \frac{R \sin\left(\alpha + \arccos\frac{R - h_s}{R}\right)}{\sqrt{R^2 - (R - h_1)^2}} \right) \\ S_t = \frac{\pi}{4} h_1 \left[\sqrt{R^2 - (R - h_1)^2} + R \sin\left(\alpha + \arccos\frac{R - h_s}{R}\right) \right] \\ S_r = \frac{\pi}{4} \sqrt{R^2 - (R - h_1)^2} \left[R \left(1 - \cos\left(\alpha + \arccos\frac{R - h_s}{R}\right) \right) - h_1 \right] \end{cases} \quad (2)$$

By defining the decomposed contact areas, the calibration model to calculate the CoF in ISF can be obtained by:

$$\mu = \mu^* - \frac{\sqrt{S_r^2 + S_t^2}}{S_z} = \frac{\sqrt{F_x^2 + F_y^2}}{F_z} - \frac{\sqrt{S_r^2 + S_t^2}}{S_z} \quad (3)$$

where the circumferential CoF can be calculated as:

$$\mu_\theta = \mu^* - \frac{S_t}{S_z} = \frac{F_t}{F_z} - \frac{S_t}{S_z} \quad (4)$$

2.3. New analytical model for predicting friction reduction under vibration

To overcome the issue of applying the Coulomb friction model in ISF due to the neglect of elastoplastic deformation on the contact surface, Gutowski and Leus [31,32] proposed dynamic prediction models to analyse the effect of vibration direction on the frictional force. The models achieved a better consistency compared with the Coulomb model, which was also validated by Wu et al. [33]. To investigate the influence of high-amplitude vibration on friction conditions in the RV-ISF process, this section proposes a new analytical prediction model of friction reduction under vibration by developing a dynamic friction model.

The traditional Coulomb model assumes that the contact surfaces are ideally rigid and smooth, so that the frictional force and CoF are constant for both surfaces at the same contact interface and contact pressure. However realistically, the contact surfaces between sheet metals are non-ideally smooth with asperities existing in the sheet surface as illustrated in Fig. 3. As a result, the sheet surfaces do not directly contact each other across the entire contact region, but rather over some randomly distributed roughness asperities.

Fig. 3 shows the contact modelling method by considering randomly-distributed roughness asperities as ‘‘micro-springs’’, and a dynamic friction model is proposed based on this contact modelling method to describe the deformation under the effect of vibration in RV-ISF. In the concept of ‘‘micro-spring’’ model, the deformable contact region consisted of the roughness asperities is assumed as an elastic damping element, MN, to characterise the tangential stiffness of the contact

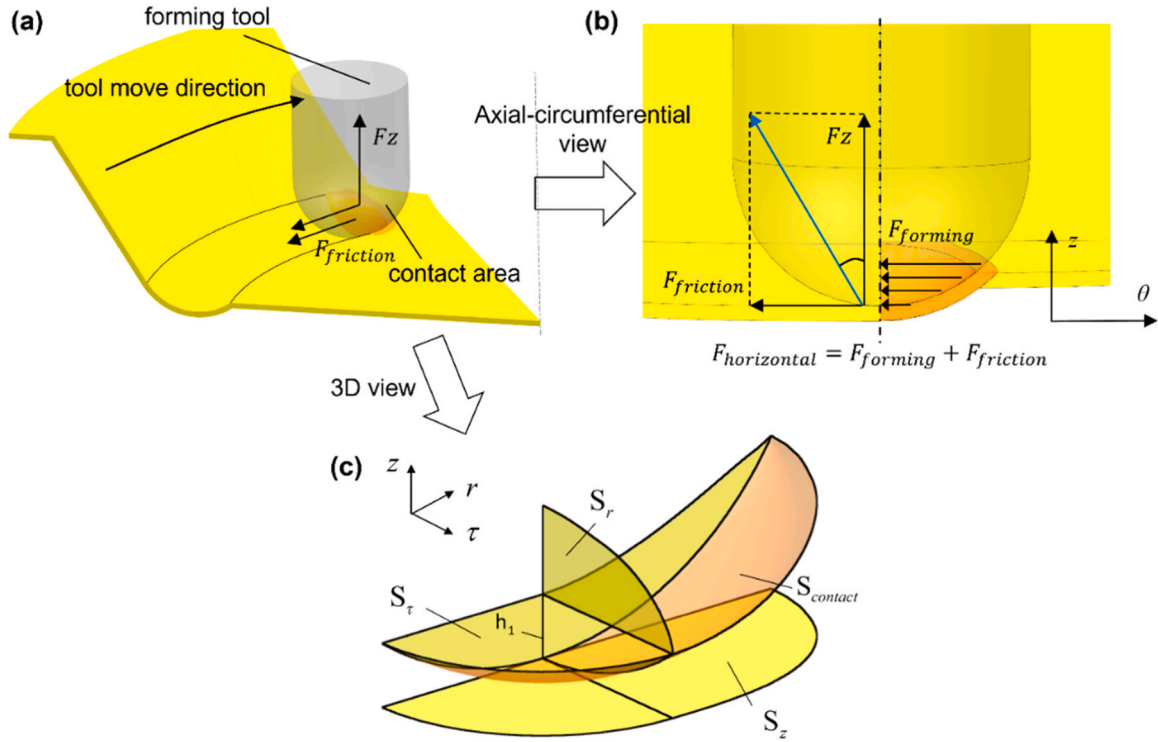


Fig. 2. Schematic of the contact area between the tool and sheet metal in incremental sheet forming. (a) Ellipsoidal contact area in incremental sheet forming. (b) Axial-circumferential view of contact area. (c) Decomposition of the contact area along the radial direction S_r and tangential direction S_r .

surface as well as the variation of elastic deformation, as shown in Fig. 3b. As the tangential force is applied by the tool, the elastic element MN deflects and moves along the tangential direction with the tool in ISF. The elastic deformation of MN is considered being related to the elastic deformation in the tangential direction, which directly determines the modulus and direction of the frictional force. After applying the vibration field, the elastic deformation of MN will then fluctuate, resulting in variations of frictional force and CoF on the contact surface. Therefore, a dynamic friction model can be developed to describe the elastic deformation of the contact surface and predict the friction reduction under vibration in the RV-ISF process, introduced in detail in the following.

The relationship between the elastic deformation of roughness asperities and frictional force is introduced by Dupont et al. [34]:

$$F_f = k_t s \quad (5)$$

where F_f is the frictional force, s represents the elastic deformation of MN along the tangential direction and k_t represents the tangential contact stiffness, which can be determined from the experimental tests of frictional force measurement.

The elastic deformation rate of roughness asperities at contact surfaces is assumed being related to the tangential stiffness as well as the relative velocity of the contact region, which can be expressed as:

$$\dot{s} = \frac{ds}{dt} = v_r \left[1 - \gamma \frac{k_t}{F_c} \text{sgn}(v_r) s \right]^\kappa \quad (6)$$

where F_c represents the frictional force without vibration in conventional ISF, which can be calculated experimentally by multiplying the vertical forming force F_z by the CoF μ defined in Eq. (3). κ determines the relationship between the tangential elastic deformation and tangential force. γ is a parameter depending on the modulus of the elastic deformation, which can be taken as 1 as investigated by Gutowski and Leus [31].

As shown in Fig. 3c, the dominated relative movements between the

sheet metal and the tool in RV-ISF include: the circumferential feed of the tool, axial rotation of the tool and radial vibration of the tool. All of the three tool movements significantly affect the value of the elastic deformation of roughness asperities, denoted as s , which dramatically affects the surface friction of the sheet metal in RV-ISF. Therefore, it is essential to calculate the value of s , in the contact region to obtain the variation of frictional force under the vibration.

The value of the elastic deformation, s , during the three relative movements of the tool can be characterised by the displacement of the end points M and N, while N' is the projection of the point N onto the surface of the sheet,

$$s(t) = \sqrt{[N'_x(t) - M_x(t)]^2 + [M_y(t) - N'_y(t)]^2} \quad (7)$$

Fig. 4 shows the variation of the elastic deformation s under the three tool movements in RV-ISF. An arbitrary contact time between the tool and the sheet can be selected as the initial time of the modelling, t , before the tool movement occurs. Since the contact area in ISF is considered as a spherical surface based on the characteristics of the tool as investigated by Chang et al. [30], the cylindrical coordinate system (ρ , θ) is adopted in this study to solve for the value of s , in the RV-ISF. The original coordinate of Point N' can be described as $N'_x = 0, N'_y = -\rho$. By taking into account the circumferential feed and axial rotation movements of the tool in the RV-ISF, Point N' moves to a new position at Point $N1'$, and the coordinates can be updated as $N1_x = \rho \sin \theta + v_d \Delta t, N1_y = -\rho \cos \theta$.

During the circumferential feeding and axial rotating of the tool, Point M moves along the path of $MN1'$ to the position $M1'$, and the modulus and direction of the elastic deformation, s , will vary during the movement. The instantaneous direction of this elastic deformation can be identified by the intersection angle of the sheet α , as shown in Fig. 4, and the variation of modulus of the elastic deformation is determined by its increment Δs . The new elastic deformation s after these movements can be updated to s_1' as:

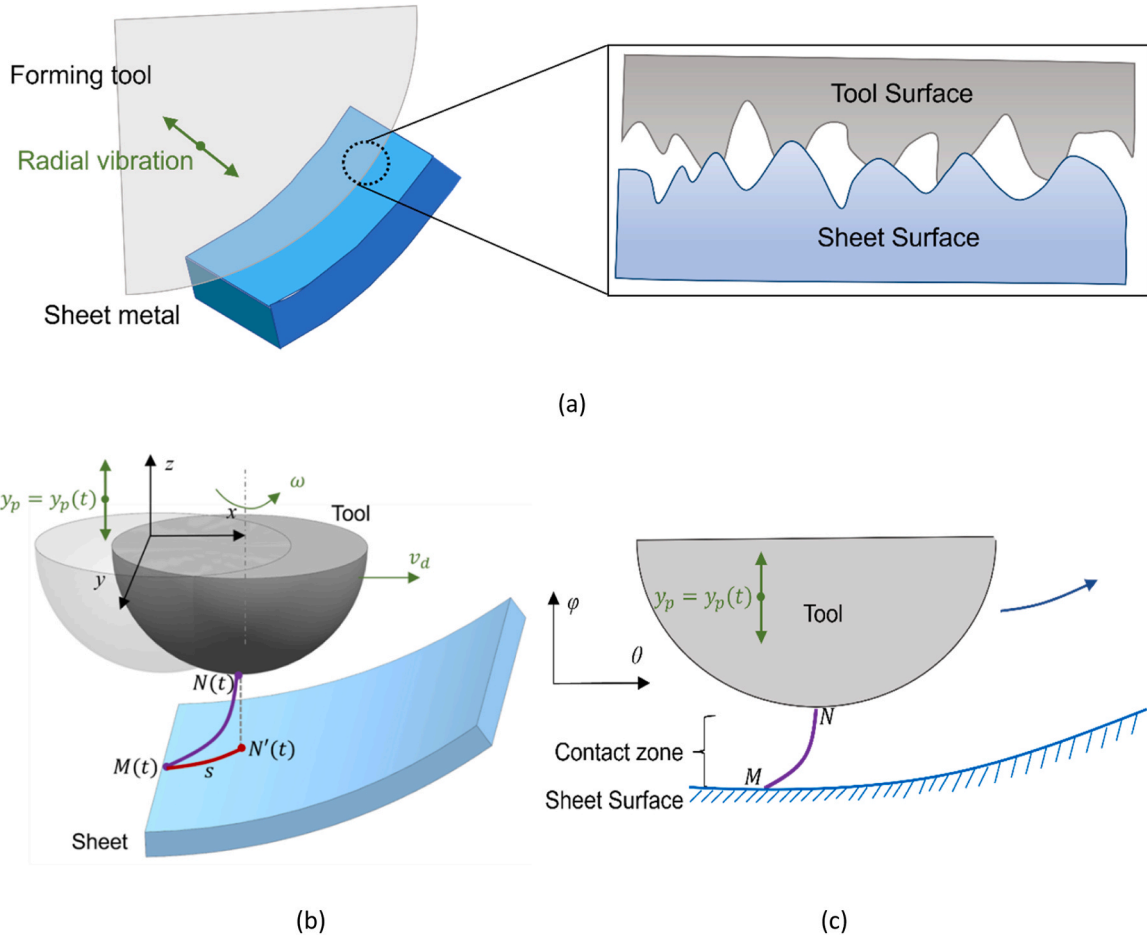


Fig. 3. Surface contact modelling considering tool relative movements in rotational vibration-assisted incremental sheet forming. (a) Micro contact between roughness asperities at the contact area. (b) Schematic of contact modelling. (c) Elastic deformation in the contact modelling.

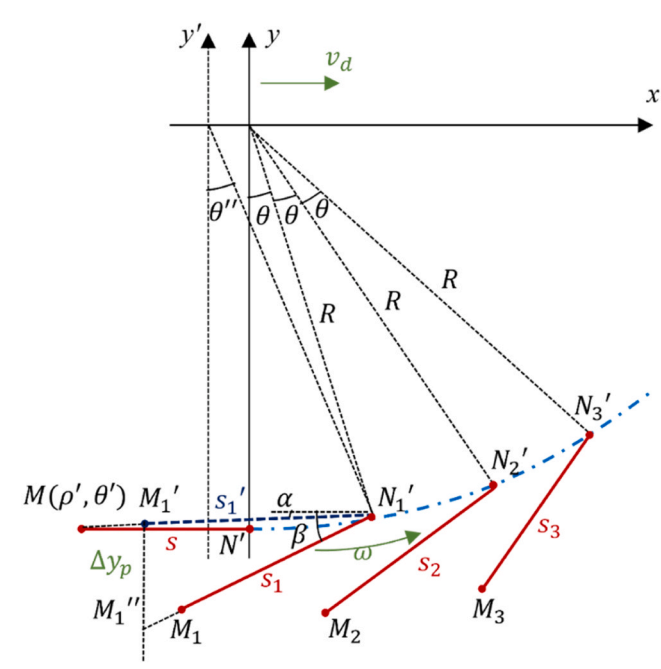


Fig. 4. Variation of elastic deformation on the contact area considering tool movements and vibration in rotational vibration-assisted incremental sheet forming.

$$s_1 = s + \Delta s = s + \nu_{r1} \left[1 - \gamma \frac{k_r}{F_c} \text{sgn}(\nu_{r1}) s \right]^\kappa \Delta t \quad (8)$$

The relative velocity ν_{r1} of the elastic deformation s can be determined by $\nu_{r1} = \frac{MN'_1 - s}{\Delta t}$, while the modulus of MN' and the corresponding angle can be calculated as $MN'_1 = \sqrt{\rho^2 + \rho^2 - 2\rho\rho'\cos(\theta + \theta'')}$, $\theta'' = \left| \arctan \frac{N'_1 x}{N'_1 y} \right|$.

After determining the modulus of the updated elastic deformation s_1' , the coordinate of the new Point M_1' , the updated Point M , can be easily calculated as $M'_1 x = N'_1 x - s_1' \cos \alpha$, $M'_1 y = N'_1 y - s_1' \sin \alpha$. While the intersection angle α can be calculated by $\sin \alpha = \frac{N'_1 y - M_y}{MN'_1}$, $\cos \alpha = \frac{N'_1 x - M_x}{MN'_1}$.

In addition to the circumferential feed and axial rotation movement in RV-ISF, the rotational-vibration tool also exerts a radial vibration field onto the sheet metal. In this work, the radial vibration movement of the tool can be assumed to conform to the Cosine law. After a period of time Δt , the vibration displacement along the radial direction generated by the tool is:

$$\Delta y_p = A \left[\cos \omega(t + \Delta t) - \cos \omega t \right] \quad (9)$$

Therefore, after the radial vibration the coordinates of the end point M will be updated to M'' as $M''_{1x} = M_{1x}$, $M''_{1y} = M_{1y} - \Delta y_p$.

After the circumferential feed, axial rotation and radial vibration at the time interval Δt , the elastic deformation of the roughness asperities changes from s_1' to s_1 as shown in Fig. 4. The direction of s_1 can be determined by the intersection angle β , and its modulus can be

calculated as:

$$s_1 = s'_1 + \Delta s_1 = s'_1 + \nu_{r2} \left[1 - \gamma \frac{k_t}{F_c} \text{sgn}(\nu_{r2}) s'_1 \right]^\kappa \Delta t \quad (10)$$

ν_{r2} is the average velocity of Point M along the line $N_1'M_1'$, and its value can be calculated by $\nu_{r2} = \frac{M_1'N_1' - s'_1}{\Delta t}$, and the modulus of MN' can be calculated as $M_1'N_1' = \sqrt{(s'_1 \cos \alpha)^2 + (s'_1 \sin \alpha + \Delta y_p)^2}$.

By determining the elastic deformation s_1 after a time interval Δt , the coordinates of the roughness asperity endpoint M_1 can be determined by $M_{1x} = N_{1x} - s_1 \cos \beta$, $M_{1y} = N_{1y} - s_1 \sin \beta$, while the intersection angle β can be obtained by $\sin \beta = \frac{\Delta y_p + s'_1 \sin \alpha}{M_1'N_1'}$, $\cos \beta = \frac{s'_1 \cos \alpha}{M_1'N_1'}$.

By determining the modulus and the direction of the elastic deformation at the current time, the instantaneous value of the frictional force can be obtained. According to the geometric relationship, the frictional force along the tangential direction can be obtained by:

$$F_{r1} = k_t s_1 \cos(-\theta'' + \beta) \quad (11)$$

The position of Point M (coordinates of Point M_1) after time interval Δt will be used as the starting point of Point M in determining the next movement period, and will be continuously updated in the next successive time intervals ($2\Delta t$, $3\Delta t$, ..., $n\Delta t$), as shown in Fig. 4. The final tangential frictional force within one vibration cycle can be obtained as:

$$\overline{F_{r1}} = \frac{1}{n} \sum_{i=1}^n F_{ri} \quad (12)$$

where n is the number of time intervals in one vibration cycle, expressed by $n = \frac{T}{\Delta t} = \frac{1}{f\Delta t}$.

Comparing the tangential frictional force after vibration, $\overline{F_{r1}}$, with the non-vibration frictional force, F_c , the average reduction ratio of the frictional force caused by vibration can be eventually obtained by the analytical model derived in the above to evaluate the friction condition using different tools in RV-ISF:

$$r = \frac{\mu_r}{\mu_c} = \frac{\overline{F_{r1}}}{F_c} \quad (13)$$

The contact rigidity k_t is obtained from the work by Gutowski and Leus [31] while F_c is obtained from the tool forces measured in the conventional ISF experiment; the details are shown in Table 1.

3. Results and discussion

3.1. Measurement results of surface roughness

Fig. 5 shows the microscopic surface profiles of the formed pyramid part shown in Fig. 1c, for AA5251 sheet material using different tools. As shown in Fig. 5a,b,c, the surface by using T0 shows obvious scratches due to the severe frictional condition. After adopting the rotational-vibration tools, the surface quality has been improved, observing bits of pitting shown on the surface by T2 and no obvious defects shown on the surface by T4. Fig. 5d,e,f demonstrates that the surface profile formed by T0 shows a ravine-shaped distribution as observed by Chang et al. [35], with roughness R_a as of $0.563\mu\text{m}$ and R_z as of $3.656\mu\text{m}$. The microscopic surface profile by T2 shows a wave-shaped distribution with R_a as of $0.486\mu\text{m}$ and R_z as of $3.192\mu\text{m}$, while that by T4 shows a uniform distribution, with R_a as of $0.469\mu\text{m}$ and R_z as of $3.382\mu\text{m}$. It indicates that due to the effect of friction reduction under vibration as reported by Xie et al. [4] and Yao et al. [5], the introduction of the vibration field creates an obvious impact on the improvement of surface quality in RV-ISF.

To further analyse the surface quality under the vibration field in the RV-ISF, Fig. 6a,b compare the surface roughness values using different tools in forming AA5251, AA6082 and AZ31B sheet materials. As shown in Fig. 6a,b, T0 produces the worst surface quality with R_a of $1.03\mu\text{m}$ and R_z of $6.5\mu\text{m}$ for AA6082, R_a of $1.775\mu\text{m}$ and R_z of $13.5\mu\text{m}$ for AZ31B. T2 improves the surface quality due to the effect of vibration friction reduction with R_a of $1.01\mu\text{m}$ and R_z of $6.05\mu\text{m}$ for AA6082, R_a of $1.725\mu\text{m}$ and R_z of $10\mu\text{m}$ for AZ31B. T4 shows the lowest roughness R_a and R_z values as shown in Fig. 6 when compared with other tools.

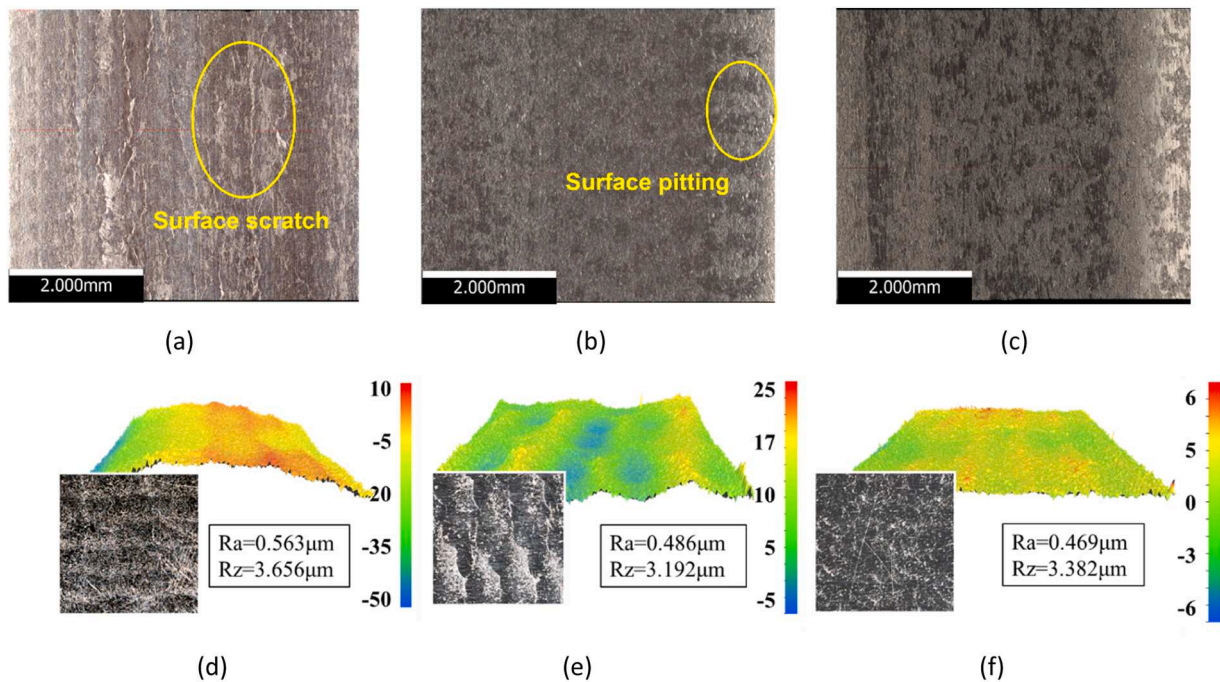


Fig. 5. Microscopic surface profiles (μm) of AA5251 material by using different tools in rotational vibration-assisted incremental sheet forming process. (a) Surface quality by T0. (b) Surface quality by T2. (c) Surface quality by T4. (d) Microscopic surface profile by T0. (e) Microscopic surface profiles by T2. (f) Microscopic surface profiles by T4.

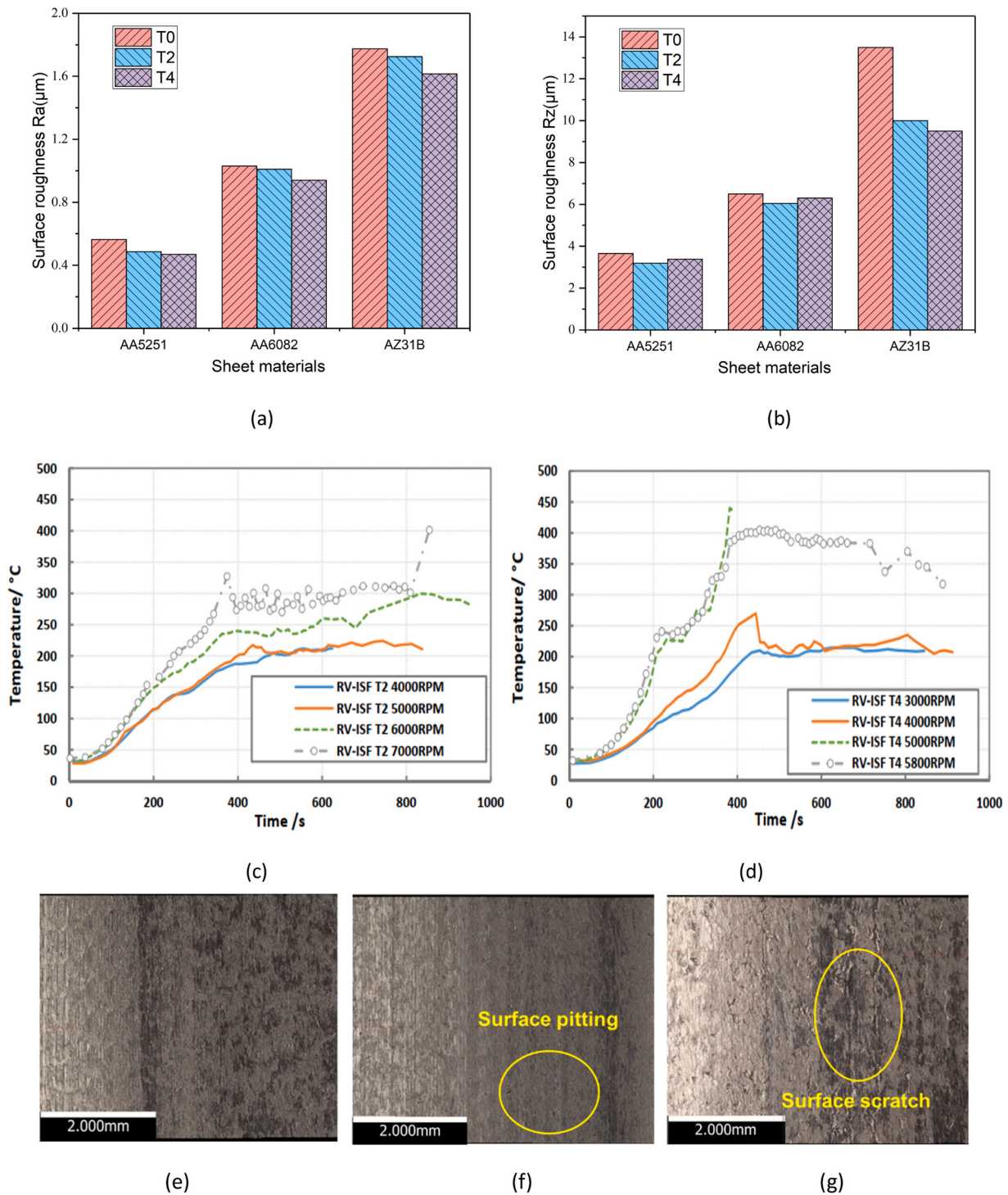


Fig. 6. Surface roughness (μm) by using different tools and sheet materials in the rotational vibration-assisted incremental sheet forming process. (a) Surface roughness R_a of AA5251, AA6082 and AZ31B using different tools. (b) Surface roughness R_z of AA5251, AA6082 and AZ31B using different tools. (c) Measured peak temperatures of AZ31B sheet by T2 tool under different rotational speeds. (d) Measured peak temperatures of AZ31B by T4 tool under different rotational speeds. (e) Surface quality of AA5251 by T4 under 4000RPM. (f) Surface quality of AA5251 by T4 under 6000RPM. (g) Surface quality of AA5251 by T4 under 7000RPM.

According to the study by Matsumoto et al. [16], the introduction of the low-frequency vibration showed its advantages in reversing the friction force vector periodically, leading to a significant decrease of the average friction force. In addition, the lubrication condition can be improved through the repeated filling of the lubricant into the contact surface between the tool and the sheet due to the offset or groove design feature in the RV-ISF tools. Especially for T4 tool with grooves, better lubrication conditions can be obtained as the lubricant can remain on the

groove gaps of T4 tool surface. It can be concluded that due to the friction reduction and lubrication improvement, the surface quality of sheet metal can be improved under the effect of low-frequency and high-amplitude vibration field by T2 and T4 tools compared with conventional ISF process.

Forming temperature, one of the important parameters affecting the surface quality, can be controlled in the RV-ISF process by adopting different rotational speeds of the tool. Fig. 6c,d show the variations of

the peak forming temperature measured by an infrared thermal camera for AZ31B material in RV-ISF process under different rotational speeds. It can be observed that the local peak temperature of the sheet obtained by T4 tool is significantly greater than that by T2 tool under the same rotational speed due to a combined effect of larger contact area and higher contact frequency between the T4 tool and sheet. Fig. 6e,f,g also show that with the increasing of tool rotational speed, the surface quality of all sheets becomes worse, and surface pitting and scratches can be observed under high rotational speeds. This is because the surface quality and friction condition of the sheet in RV-ISF are not only affected by temperature but also by the shearing stress of the sheet surface induced by the tool under different rotational speeds. An increased rotational speed, thus a greater contact frequency, not only elevates the surface temperature but also increases the shearing stress of the sheet surface, both increasing the damage of the surface material.

The amplitude and frequency of the vibration fields generated by using different rotational-vibration tools vary significantly, resulting in the distinct difference of friction reduction effect. Fig. 7 shows the experimentally measured amplitudes and frequencies of the vibration field generated by the different tools in the RV-ISF experiments. The dominated frequencies and amplitudes at tool rotational speed of 2000 RPM and 3000 RPM by using T2 tool are 68 Hz, 82 μm and 102 Hz, 65 μm respectively; while for T4 tool, the dominated frequencies and amplitudes are 137 Hz, 11 μm and 203 Hz, 4 μm respectively. Vibrations at other frequencies are not considered in this work.

3.2. Microstructure characterisation

To investigate the influence of vibration on the microstructure of the sheet thickness after the deformation, Fig. 8 shows the electron back-scattered diffraction (EBSD) and Vickers hardness results of AZ31B parts formed by different tools in RV-ISF. It has been observed that the average grain size of the parts formed by different tools are similar (about 2.7 μm) as shown in Fig. 8a,b, but the proportion of low-angle grain boundaries (LAGBs) by T2 as 14.8 % is much smaller compared with that by T0 of 25.6 % and T4 of 25.4 % as shown in Fig. 8d. It can be also observed that the mean value of Kernel Average Misorientation (KAM) under T2 is notably smaller compared to that under T0 and T4, and a considerable improvement of the Vickers micro-hardness on surface material can be found by using T2 and T4. Fujiyama et al. [36] adopted the variation law of KAM values among multiple grains to track the dislocation movement in heat resistant steels. It was suggested that KAM could be regarded as a qualitative description of geometrically necessary dislocation (GND) density distribution in metallic materials expressed by [37]:

$$\rho_{\text{GND}} \approx \frac{\theta\beta}{\mu b} \quad (14)$$

where θ , μ , β and b represent the mean KAM value, step size for EBSD scanning, material constant and Burgers vector, respectively. Based on this expression, the GND densities for T0, T2 and T4 can be calculated as 19.74×10^3 , 15.2×10^3 and $26.2 \times 10^3 \mu\text{m}^{-2}$ respectively, demonstrating that the dislocation density by T2 is the lowest compared to those by T0 and T4.

When the same level of plastic deformation is produced for the sheet material by T0, T2 and T4 tools, the grain size of the material stays basically the same. It can be considered that the energy from a high-amplitude vibration field is not absorbed by the stable high-angle grain boundaries (HAGBs), therefore the grain size does not vary significantly by using different tools. While adopting the T4 tool with lower vibration amplitude than that by T2 tool, the elastic deflection occurs primarily on the sheet material. The vibration energy exerted by T4 cannot be effectively transferred to the plastic deformation area of the sheet, resulting in the insignificant decrease of the dislocation density, as shown in Fig. 8c. However, once the high-amplitude vibration field exerted by T2 tool is created to the plastic deformation area of the sheet, greater vibration energy can be preferentially absorbed by LAGBs and the dislocations inside the crystal. Moreover, the contact probability of the heterozygous dislocations can be significantly increased by the high-amplitude vibration field from the T2 tool, leading to intensified dislocation annihilation and reduction of dislocation density, as shown in Fig. 8c.

As investigated by Lin et al. [12] and Meng et al. [13], the application of high-amplitude vibrations to the material surface promoted the contact probability of the heterozygous dislocations and dislocation annihilation within the crystal, resulting in a significant decrease of sub-grain boundaries and LAGBs within the material, as shown in Fig. 8d. Moreover, the vibration energy is preferentially absorbed by the dislocations and LAGBs, and LAGBs after absorbing the vibration energy are prone to be transformed into high-angle grain boundaries under the effect of a high-amplitude vibration field. Therefore, the micro-hardness of sheet surface increases with the increasing of the vibration amplitude, as shown in Fig. 8d, which is beneficial to improving friction condition on the contact area and surface quality [38–40]. As a significant mechanism, different from the friction reduction and lubrication improvement under vibration, the increased hardness of surface material by applying the high-amplitude vibration field can further improve the friction condition and surface quality in the RV-ISF process.

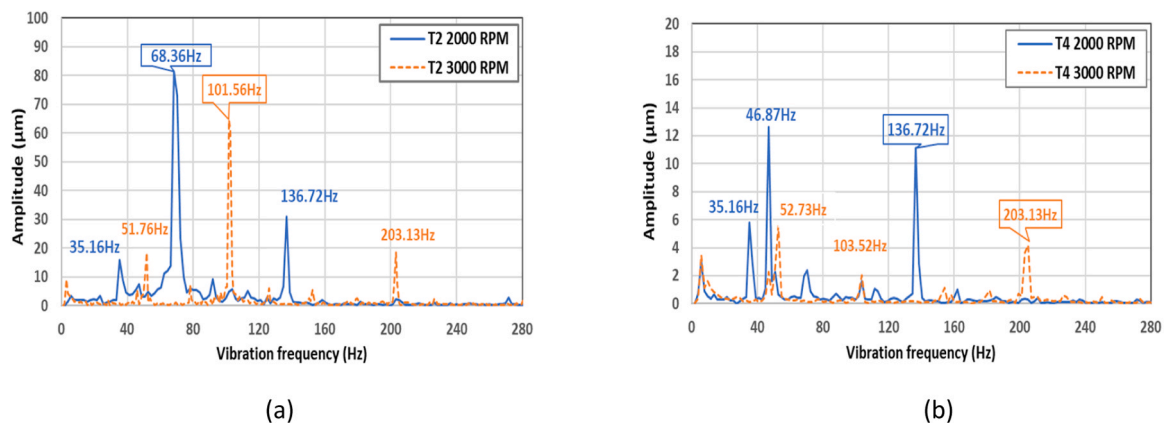


Fig. 7. Measurement of vibration frequencies and amplitudes for AA5251 in rotational vibration-assisted incremental sheet formed by T2 tool, (a) and by T4 tool, (b).

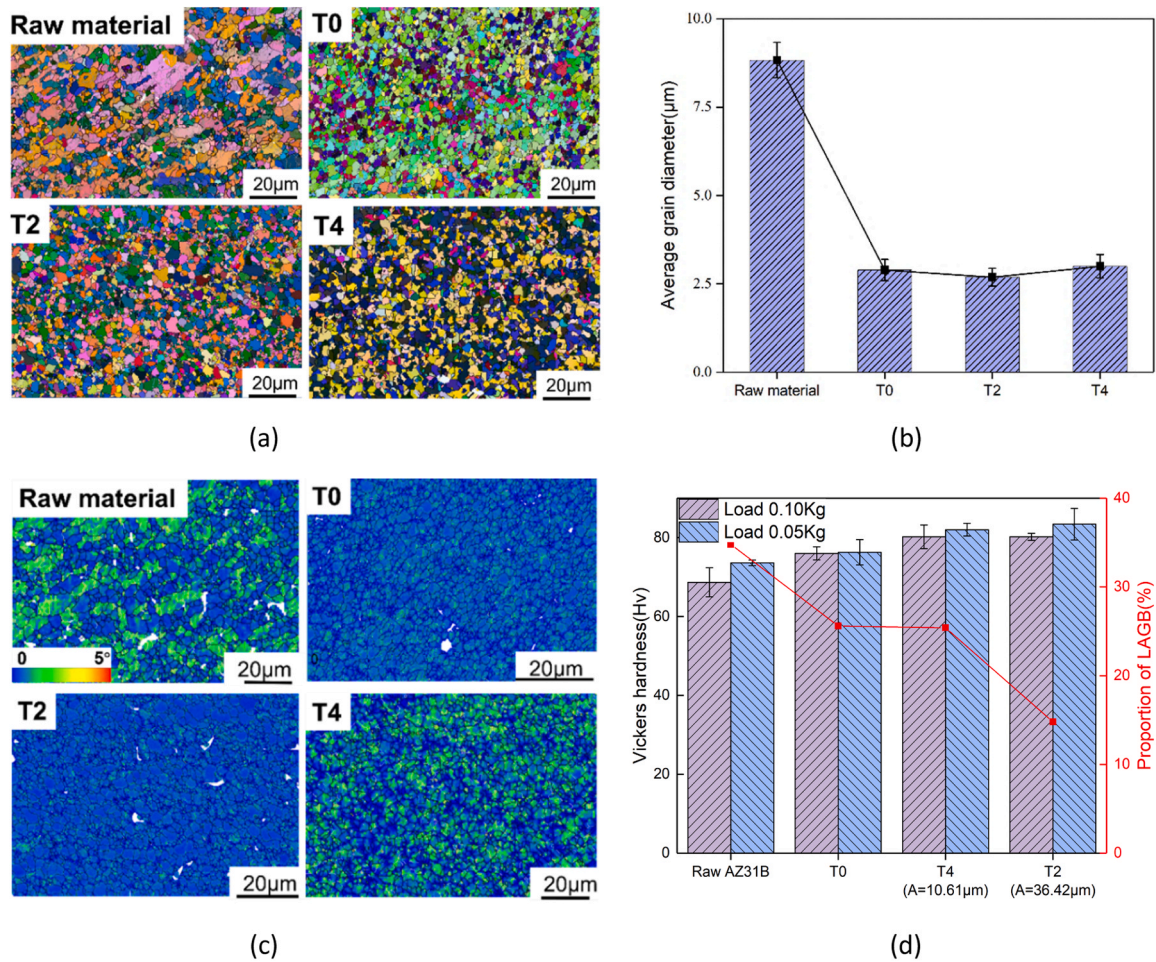


Fig. 8. Comparison of microstructures of AZ31B sheet thickness using different tools in rotational vibration-assisted incremental sheet forming process. (a) All Euler figures of material of the sheet metal by T0, T2 and T4 tools. (b) Grain sizes by T0, T2 and T4 tools. (c) Kernel Average Misorientation result of sheet metal by T0, T2 and T4 tools. (d) Measured sheet surface micro-hardness and low-angle grain boundary percentage by T0, T2 and T4 tools.

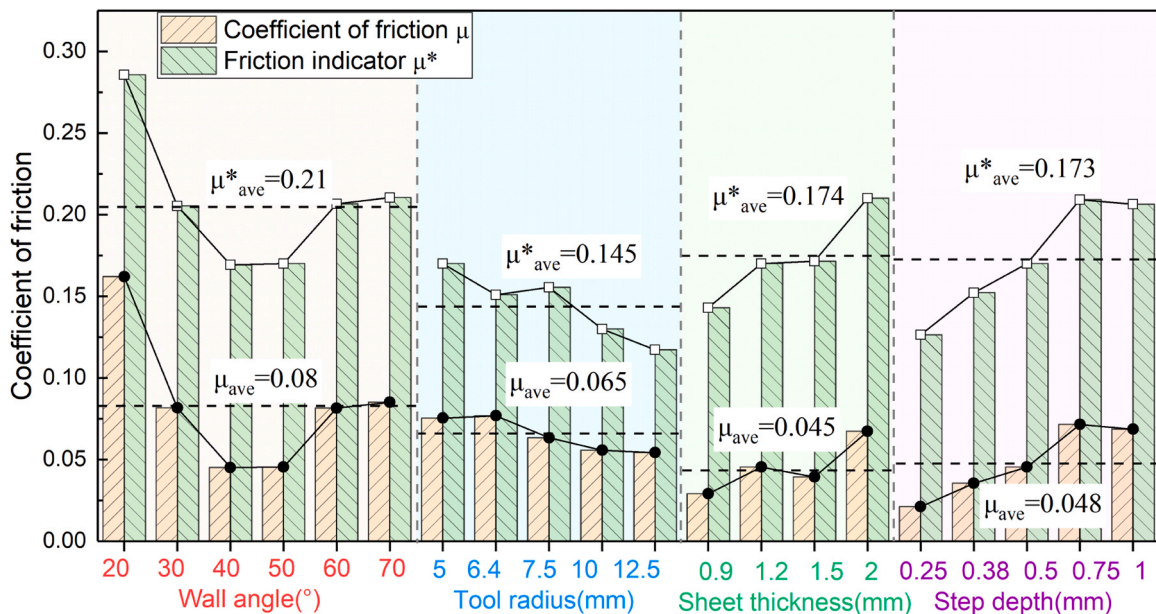


Fig. 9. Comparison of coefficient of friction calculated by the developed calibration model with friction indicator under different process parameters.

3.3. Coefficient of friction

Fig. 9 shows the CoF μ calculated by using the developed calibration model (Eq. (3)) from the ISF experimental data reported by Aerens et al. [41], and compared with the value of friction indicator μ^* . It can be found that the variation trends of μ and μ^* under different process parameters are basically the same. μ and μ^* increase with the increasing of sheet thickness and step depth, and are inversely proportional to the tool radius. Furthermore, μ and μ^* show a nonlinear relationship with the wall angle, and reach the minimum value at the wall angle of 40° to 50° . By comparing the strain evolution obtained from FE simulations with that measured through DIC equipment during ISF experiments for AA3103 material, Eyckens et al. [42] found that the CoF μ from the conventional ISF experiment was approximately 0.05, while the value of the friction indicator μ^* exceeded this value considerably. The friction indicator μ^* overestimates the friction effect of the tool in ISF because it incorrectly includes the horizontal forming force into the frictional force. After excluding the effect of the horizontal forming force in the developed calibration model, the CoF μ , varying between 0.03 and 0.08, is close to the experimentally measured value of 0.05. Therefore, this new calibration model can truly reflect the effect of the friction on surface quality in ISF, and provides an essential tool for calculating CoF for further investigating friction conditions when using different tools in the RV-ISF process.

4. Experimental validation of new analytical friction model

To verify the proposed analytical model of friction reduction due to vibration, a series of conventional ISF and RV-ISF experiments using different tools for different sheet materials are conducted. Furthermore, based on this analytical model, the influences of tool rotational direction and process parameters on the friction reduction in RV-ISF are discussed and analysed.

4.1. Analysis of friction reduction due to vibration

Fig. 10 shows the experimentally measured horizontal and vertical forces in forming geometries with varying wall angles (Fig. 1c) using different tools (Fig. 1b). In addition to the RV-ISF experiments, series of experimental tests of conventional incremental sheet forming (CISF) without vibration effect as well as friction stir incremental sheet forming (FSISF) with the rotation of the tool are also conducted to demonstrate the vibration effect. As shown in Fig. 10a,c,e, the forming force of the tool is closely related to the material strength, which increases with the flow stress under the same process parameters. It can be observed that the forming force of AA6082 is the largest using different tools, followed by AA5251 with lower strength, and AZ31B has the lowest forming force because of the significantly increased forming temperatures as shown in Fig. 6c,d. It can be also seen that for different materials, the horizontal and vertical forming forces in RV-ISF by using T4 tool are significantly lower compared to that in CISF and FSISF, which is caused by the reduction of material stress due to the vibration softening effect. In addition, the horizontal and vertical forming forces by using T2 tool are the lowest compared with other tools due to the combination of the ellipsoidal shape of tool head and the distinct vibration softening effect under higher vibration amplitudes.

By employing the developed calibration model of CoF proposed in Section 2, the accurate CoFs in CISF, FSISF and RV-ISF processes can be calculated through the experimental force data, as shown in Fig. 10b, d, f. It can be seen that the calculated CoFs by the calibration model is much smaller than the CoFs by the Coulomb friction model in Fig. 9, due to the fact that the calibration model excludes the effect of the horizontal forming force on CoF to accurately describe the frictional condition. The wall angle of the geometries in Fig. 1c increases gradually with the increasing forming depth, thus the influence of wall angle on CoF can be evaluated through the varied-angle geometries. It can be found that the

CoF increases dramatically as the wall angle increases, which is caused by the increased contact area under larger wall angle. As shown in Fig. 10b, d, f, the CoF between the tool and sheet increases with increasing material hardness due to higher strength, and the CoF on the AA6082 surface is greater than other two materials. It can be also observed that the CoF can be reduced significantly by using T2 and T4 tools compared with that by T0, with the improvement of surface quality shown in Fig. 5, which is caused by the effect of friction reduction under vibration. Furthermore, it can be seen from Fig. 10b, d, f that the CoF by T2 tool with higher vibration amplitudes is much smaller than that by T4 tool for different sheet materials, indicating that the friction reduction effect by vibration with higher amplitudes becomes more pronounced.

Fig. 11 shows the analytical results of the friction reduction ratio due to the effect of vibration in RV-ISF for three materials AA5251, AA6082 and AZ31B, and compared with the experimentally obtained ratio of CoF using T2 and T4 to CoF using T0. Although the CoF increases with the wall angle, the friction reduction ratio caused by vibration remains the same and largely unchanged during the forming process, indicating that the friction reduction effect is primarily affected by the vibration amplitude rather than the wall angle. As shown in Fig. 11, the average prediction errors (%) between the analytical model and experimental results for different materials are 7.5 % by T2 and 12.68 % by T4. Therefore, it is considered that the proposed analytical model of friction reduction under vibration shows a good accuracy in predicting the friction reduction for different vibration tools and materials.

4.2. Analytical evaluation of friction behaviour

The proposed analytical friction model can be used to analyse the influence of the tool rotational direction on the friction condition in RV-ISF. Similar to the definition in machining process [43], in this study the forming procedure keeping the tool rotating in the same direction as the feed direction is defined as “down-milling”, and the opposite is named as “up-milling”. Fig. 12a,b show the variation of the elastic deformation of roughness asperities, s , during “down-milling” and “up-milling” forming procedures, respectively. Due to the difference in the rotational direction and vibration direction in “down-milling” and “up-milling”, the variation trend of the elastic deformation s is slightly different. By comparing the elastic deformation between different rotational directions shown in Fig. 12c, there is no obvious difference of elastic deformation in the initial stage, demonstrating that the impact of the vibration field on the surface friction is not instantaneous, but takes a certain time to take place. The elastic deformation s fluctuates in the later stage within one vibration cycle, and the fluctuation in the “down-milling” becomes significantly greater than that in the “up-milling”. Ultimately, the friction reduction effect under vibration caused by the “down-milling” procedure is also significantly greater than that by the “up-milling” procedure under the same process parameters in the RV-ISF, indicating that the “down-milling” procedure is more effective for improved friction condition and surface quality than that by employing the “up-milling” procedure. The experimental results of AA6082 sheets in Fig. 12d also indicates that the surface quality of the “up-milling” formed part with R_a of $1.11\mu\text{m}$ is worse than that of the “down-milling” formed part with R_a of $0.78\mu\text{m}$. Consistent with the conclusion from the milling process in [43], significant scratches can be seen on the surface of the “up-milling” part while they are not visible on the “down-milling” part surface, suggesting that the “down-milling” procedure in the RV-ISF can achieve a greater friction reduction under vibration leading to a better surface quality compared with the “up-milling” procedure.

The influence of major parameters on the friction reduction under vibration effect can also be evaluated by the developed analytical friction model, as shown in Fig. 13. The friction reduction effect under vibration is directly proportional to vibration amplitude and non-vibration friction force F_c , and maintains inversely proportional to the tool radius and the contact rigidity coefficient kt . The rotational speed

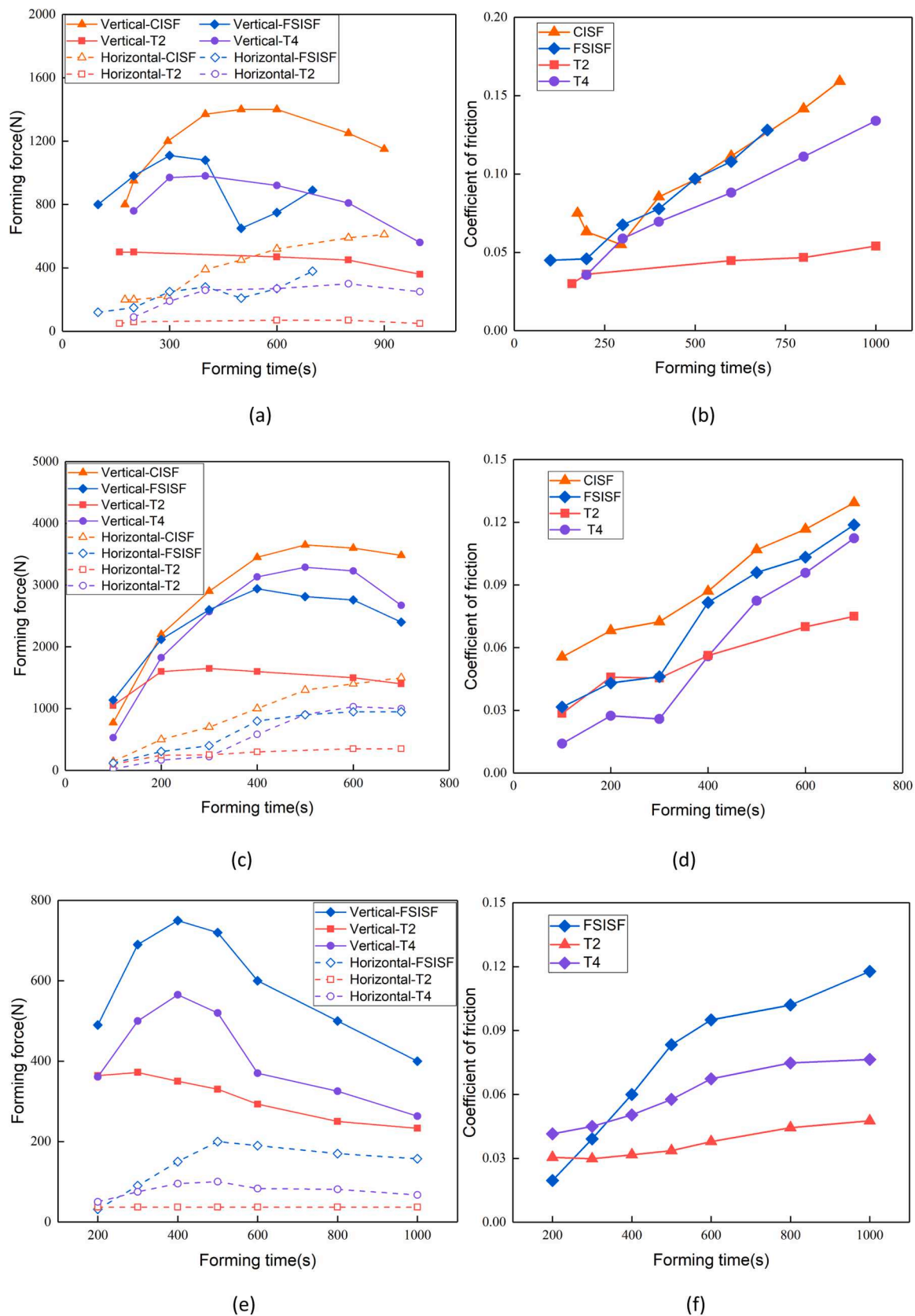
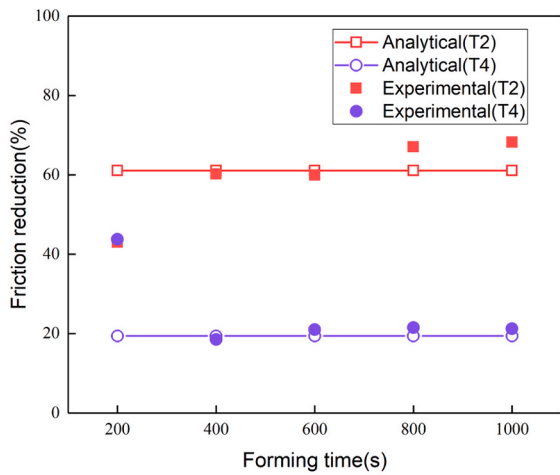
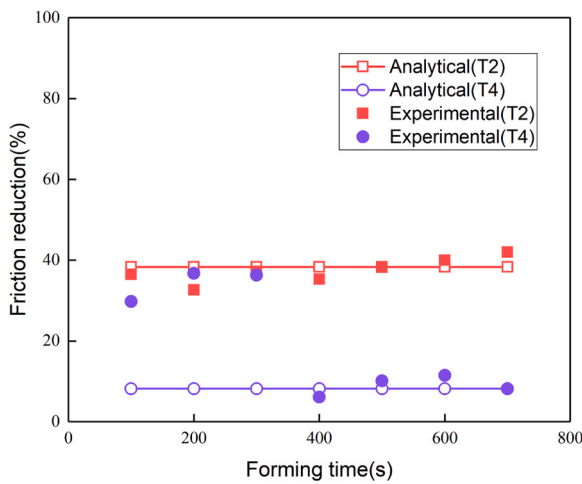


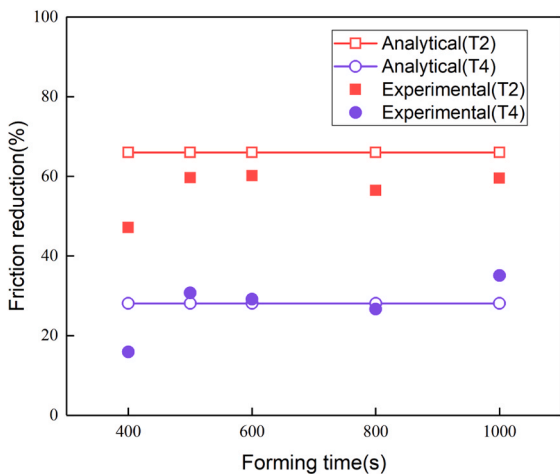
Fig. 10. Measured experimental forming forces and calculated coefficient of friction of different materials by using different tools. (a) Horizontal and vertical forming forces for AA5251. (b) Coefficient of friction for AA5251. (c) Horizontal and vertical forming forces for AA6082. (d) Coefficient of friction for AA6082. (e) Horizontal and vertical forming forces for AZ31B. (f) Coefficient of friction for AZ31B.



(a)



(b)



(c)

Fig. 11. Comparison of measured experimental and predicted results of friction reduction by using different tools. (a) Reduction of coefficient of friction for AA5251 by T2 and T4 tools. (b) Reduction of coefficient of friction for AA6082 by T2 and T4 tools. (c) Reduction of coefficient of friction for AZ31B by T2 and T4 tools.

and feed rate of the tool have little effect on the friction reduction, but still have obvious influence on the surface quality through changing the surface wear rate between the tool and sheet contact. It can be concluded that the vibration amplitude shows the greatest effect on friction reduction effect, followed by non-vibration friction force F_c and contact rigidity coefficient k_t , which are mainly determined by material properties, and finally by the tool radius. For a specific material, the contact rigidity coefficient k_t and non-vibration friction force F_c are essentially constant, so that the friction reduction effect under vibration can be enhanced by increasing the vibration amplitude and decreasing the tool radius, to further improve the surface quality of the RV-ISF parts.

4.3. Finite element analysis of friction behaviour

To further validate two friction models developed and evaluate the vibration effect on surface quality in the RV-ISF, finite element (FE) models are established to simulate the RV-ISF process in forming the pyramid geometry with constant wall angle shown in Fig. 1c by using Dynamic Explicit in ABAQUS FE software. von Mises yield criterion and coupled temperature-displacement shell elements with five integral points through thickness are used in simulating the RV-ISF AA6082 sheet metal with step depth of tool path as 0.3 mm and sheet thickness as 1 mm. T0, T2 and T4 tools are modelled as rigid bodies in the FE simulation. The CoF on the contact surface between the sheet metal and the tool is taken as 0.12, 0.05 and 0.09 for using T0, T2 and T4, respectively, thus the accuracy of the friction indicator by Coulomb model and the CoF by the calibration model could be quantitatively compared. The simulated pyramid part after RV-ISF is shown in Fig. 14a, and a node at the inclined region is selected for the analysis of friction condition and vibration effect.

As shown in Fig. 14b, the simulated forming forces along the vertical and horizontal directions agree with the experimental results, validating the accuracy of the FE simulation model. Furthermore, Fig. 14c shows the simulated radial displacement of the selected node, and the simulated vibration amplitude by using different tools can be calculated according to the same method used in the RV-ISF experiments presented in Section 4.2. Due to the step setting in Dynamic Explicit FE method it is difficult to simulate high vibration frequencies, there is a difference in the vibration frequency and amplitude between the FE simulated and experimental results. However, it can be observed that the maximum simulated vibration amplitude of 169 μm by T2 tool is significantly greater than that of 101 μm by T4 tool, which is qualitatively consistent with the experimental conclusion. Fig. 14d shows the circumferential displacement of the selected node of the deforming sheet using different tools, and the variation of the circumferential displacement corresponds to the twisting of the sheet surface material as investigated by Chang et al. [44]. As shown in Fig. 14d, the absolute value of the circumferential displacement using T2 and T4 are 0.26 mm and 0.55 mm respectively, smaller than that of 0.59 mm under T0. The decreasing of the circumferential displacement by T2 and T4 indicates that the twisting of the surface material can be suppressed by the rotational-vibration tools, especially for T2 tool.

Fig. 14e shows the simulated CoFs under different tools calculated by the Coulomb model and developed calibration model. The simulated value of the friction indicator by the Coulomb model is much larger than the CoFs by applying the calibration model, and a significant fluctuation of the CoF by T2 tool can be observed due to the vibration effect in RV-ISF. As discussed in Section 3, this overestimation of the friction indicator by the Coulomb model is caused by including the horizontal forming force in the calculation of the frictional force. However as shown in Fig. 14e, the CoFs obtained by the calibration model using T0, T2 and T4 tools are about 0.12, 0.05 and 0.09, respectively, which is consistent with the setting value of CoFs in the FE simulation models. Therefore, the evaluation method of the friction indicator using the Coulomb model is inaccurate to assess the friction condition in ISF, but

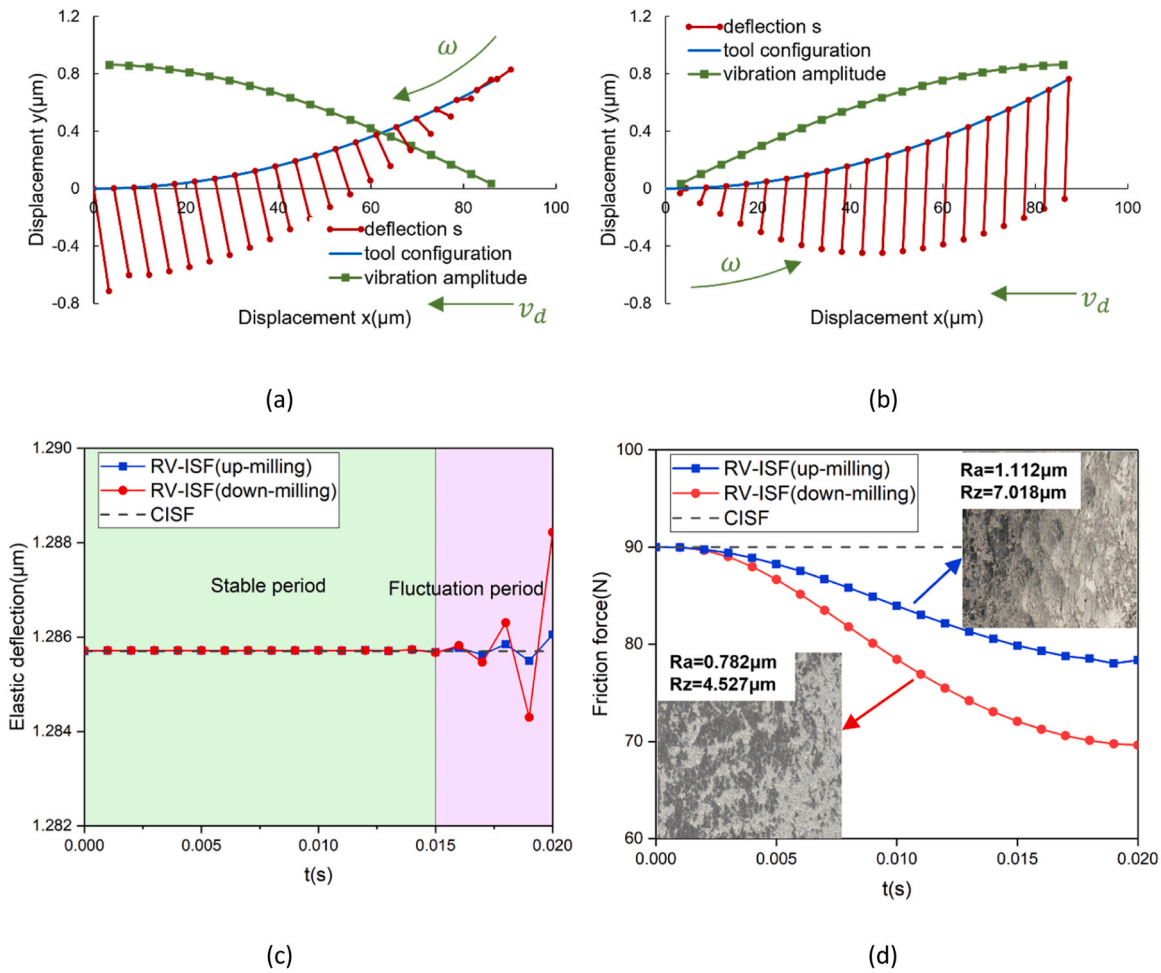


Fig. 12. Effect of "up-milling" and "down-milling" forming procedure on surface quality of AA6082 sheets in rotational vibration-assisted incremental sheet forming. (a) Elastic deformation during "down-milling". (b) Elastic deformation during "up-milling". (c) Variation of elastic deformation under the effect of vibration field. (d) Variation of frictional force under the effect of vibration field.

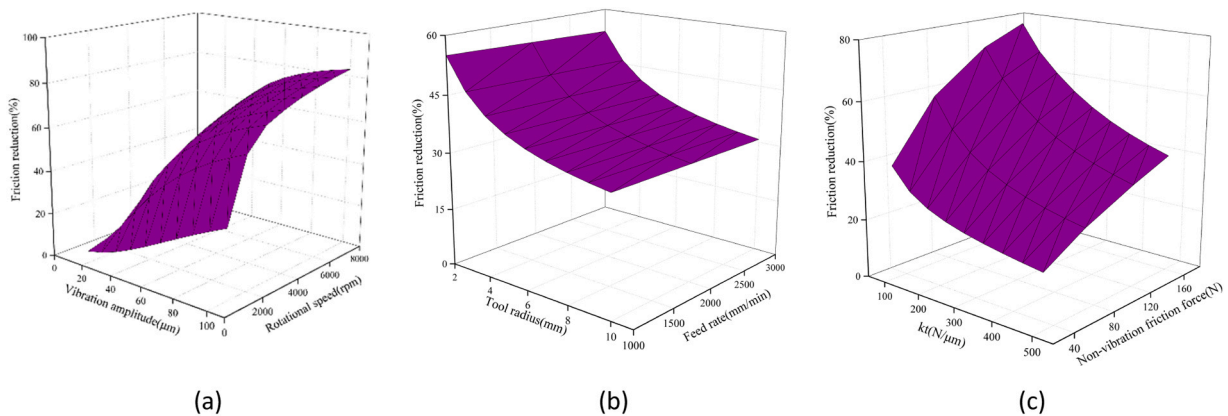


Fig. 13. Evaluation of friction reduction under different process parameters by using the analytical friction model. (a) Under different vibration amplitude and rotational speed. (b) Under different tool radius and feed rate. (c) Under different contact rigidity coefficient and non-vibration friction force.

the proposed calibration model provides an accurate evaluation method for evaluating CoF, which is applicable for the assessment of friction behaviour in different ISF process variants.

5. Conclusions

In this study, the friction condition and surface quality in the

rotational vibration-assisted incremental sheet forming (RV-ISF) process are investigated through experiments, analytical modelling, FE simulation and microstructure characterisation. Importantly, a new calibration model for calculating CoF in various ISF processes and a new analytical model for predicting friction reduction under vibration in the RV-ISF process are developed and validated, focusing on the evaluation of several underpinning mechanisms leading to the improved surface

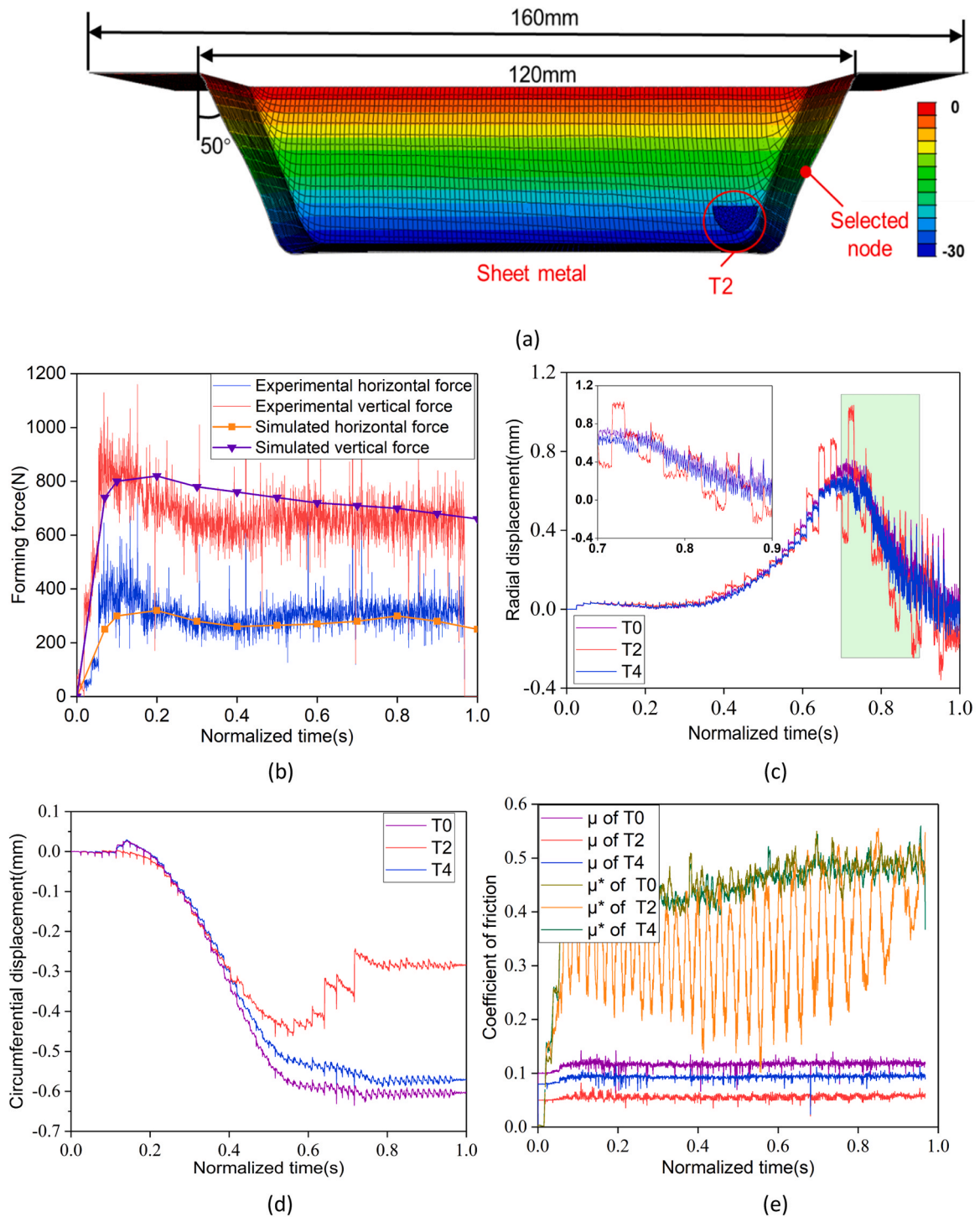


Fig. 14. FE simulation results of rotational vibration-assisted incremental sheet forming AA6082. (a) FE formed pyramid part. (b) Comparison of experimental and simulated forming forces by T4 tool. (c) Comparison of radial displacement of the selected node by different tools. (d) Simulated circumferential displacement by different tools. (e) Simulated friction indicator and coefficient of friction by using the calibration model.

quality. The main conclusions are summarised as follows:

1) By introducing a high-amplitude vibration field, considerable improvements in the surface quality of different materials can be obtained by rotating the shaped tool in the RV-ISF process. Furthermore, the underpinning mechanisms of surface improvement under vibration effect are identified and validated, including the friction reduction effect under vibration, improved lubrication condition and increased micro-hardness of the sheet surface. The

transformation of low-angle grain boundaries into stable high-angle grain boundaries caused by the vibration field increases the micro-hardness of the sheet surface in the RV-ISF process, further improving the friction condition.

2) A new calibration model for calculating CoF in ISF is proposed by excluding the effect of the horizontal forming force of the tool. Compared with the conventional concept of the friction indicator, the CoF calculated by this new method, fully validated by the experimental and FE modelling results, reflects the friction condition

in ISF with a satisfactory precision. It provides an accurate calculation method of coefficient of friction based on the unique forming characteristic of ISF, which is applicable for the assessment of friction behaviour in different ISF process variants.

- 3) A new analytical model for predicting friction reduction under vibration is developed in this study. It not only provides a new method for accurately assessing the friction condition under vibration but also enables detailed evaluations of influences of key ISF process parameters on the surface quality. Though this analytical model is developed for considering the vibration effect in RV-ISF, it is applicable for improving surface quality for other vibration assisted sheet forming processes, such as ultrasonic vibration or high-amplitude mechanical vibration fields.
- 4) T2 tool introduces the vibration field with higher amplitudes, leading to the obvious decreasing CoF compared with T4 tool. The vibration amplitude has the greatest influence on friction reduction; other variables including non-vibrating frictional force, contact rigidity coefficient and tool radius also have significant influence. These results provide new insights into how vibration parameters can be optimised for different sheet materials to reduce friction and improve surface quality, for future potential applications of the ISF technology.

CRediT authorship contribution statement

Wenxuan Peng: Methodology, Investigation, Formal analysis. **Zhi-dong Chang:** Writing – original draft, Visualization, Validation, Methodology, Investigation, Formal analysis. **Hui Long:** Writing – review & editing, Supervision, Methodology, Funding acquisition.

Declaration of Competing Interest

The authors declare that there is no conflict of interests regarding the publication of this work.

Acknowledgments

The authors wish to acknowledge the funding support received from the UK EPSRC through project grants EP/W010089/1 and EP/T005254/1. The authors would also like to acknowledge the contribution from Jamie Booth of the Department of Mechanical Engineering in the development of the new tools and RV-ISF experiment as well as performing experimental testing and supporting data measurements.

References

- [1] Sedaghat, H., Xu, W., Zhang, L., 2019. Ultrasonic vibration-assisted metal forming: constitutive modelling of acoustoplasticity and applications. *J. Mater. Process. Technol.* 265, 122–129. <https://doi.org/10.1016/j.jmatprotec.2018.10.012>.
- [2] Lin, J., Li, J., Liu, T., Zhu, L., Chu, X., Zhao, G., Guan, Y., 2021. Evaluation of friction reduction and frictionless stress in ultrasonic vibration forming process. *J. Mater. Process. Technol.* 288, 116881. <https://doi.org/10.1016/j.jmatprotec.2020.116881>.
- [3] Zhou, H., Cui, H., Qin, Q.H., 2018. Influence of ultrasonic vibration on the plasticity of metals during compression process. *J. Mater. Process. Technol.* 251, 146–159. <https://doi.org/10.1016/j.jmatprotec.2017.08.021>.
- [4] Xie, Z., Guan, Y., Zhu, L., Zhai, J., 2018. Investigations on the surface effect of ultrasonic vibration-assisted 6063 aluminum alloy ring upsetting. *Int. J. Adv. Manuf. Tech.* 96, 4407–4421. <https://doi.org/10.1007/s00170-018-1611-z>.
- [5] Yao, Z., Kim, G.Y., Faidley, L., Zou, Q., Mei, D., Chen, Z., 2012. Effects of superimposed high-frequency vibration on deformation of aluminum in micro/meso-scale upsetting. *J. Mater. Process. Technol.* 212, 640–646. <https://doi.org/10.1016/j.jmatprotec.2011.10.017>.
- [6] Bai, Y., Yang, M., 2016. The influence of superimposed ultrasonic vibration on surface asperities deformation. *J. Mater. Process. Technol.* 229, 367–374. <https://doi.org/10.1016/j.jmatprotec.2015.06.006>.
- [7] Pohlman, R., Lehfeldt, E., 1966. Influence of ultrasonic vibration on metallic friction. *Ultrasonics* 4, 178–185. [https://doi.org/10.1016/0041-624X\(66\)90244-7](https://doi.org/10.1016/0041-624X(66)90244-7).
- [8] Wang, P., Ni, H., Wang, R., Li, Z., Wang, Y., 2016. Experimental investigation of the effect of in-plane vibrations on friction for different materials. *Tribol. Int.* 99, 237–247. <https://doi.org/10.1016/j.triboint.2016.03.021>.
- [9] Wan, W., Lv, P., Liu, F., Xu, L., Bai, W., Han, G., 2023. Evaluation of interfacial friction characteristics in multi-mode ultrasonic vibration assisted micro-extrusion process. *J. Manuf. Process.* 88, 12–21. <https://doi.org/10.1016/j.jmapro.2023.01.033>.
- [10] Hung, J.C., Tsai, Y.C., 2013. Investigation of the effects of ultrasonic vibration-assisted micro-upsetting on brass. *Mater. Sci. Eng. A* 580, 125–132. <https://doi.org/10.1016/j.msea.2013.04.074>.
- [11] Ali, S., Hinduja, S., Atkinson, J., Bolt, P., Werkhoven, R., 2008. The effect of ultra-low frequency pulsations on tearing during deep drawing of cylindrical cups. *Int. J. Mach. Tool. Manuf.* 48, 558–564. <https://doi.org/10.1016/j.jmachtools.2007.06.013>.
- [12] Meng, D., Zhao, X., Zhao, S., Han, Q., 2019. Effects of vibration direction on the mechanical behavior and microstructure of a metal sheet undergoing vibration-assisted uniaxial tension. *Mater. Sci. Eng. A* 743, 472–481. <https://doi.org/10.1016/j.msea.2018.11.115>.
- [13] Lin, J., Pruncu, C., Zhu, L., Jiao, L., Zhai, Y., Chen, L., Guan, Y., Zhao, G., 2021. Deformation behavior and microstructure in the low-frequency vibration upsetting of titanium alloy. *J. Mater. Process. Technol.* 299, 117360. <https://doi.org/10.1016/j.jmatprotec.2021.117360>.
- [14] Maeno, T., Osakada, K., Mori, K., 2011. Reduction of friction in compression of plates by load pulsation. *Int. J. Mach. Tool. Manuf.* 51, 612–617. <https://doi.org/10.1016/j.jmachtools.2011.03.007>.
- [15] Behrens, B.A., Meijer, A., Stangier, D., Hübner, S., Biermann, D., Tillmann, W., Rosenbusch, D., Müller, P., 2020. Static and oscillation superimposed ring compression tests with structured and coated tools for Sheet-Bulk Metal Forming. *J. Manuf. Process.* 55, 78–86. <https://doi.org/10.1016/j.jmapro.2020.04.007>.
- [16] Matsumoto, R., Jeon, J.Y., Utsunomiya, H., 2013. Shape accuracy in the forming of deep holes with retreat and advance pulse ram motion on a servo press. *J. Mater. Process. Technol.* 213, 770–778. <https://doi.org/10.1016/j.jmatprotec.2012.11.023>.
- [17] Zhang, Q., Ben, N., Yang, K., 2017. Effect of variational friction and elastic deformation of die on oscillating cold forging for spline shaft. *J. Mater. Process. Technol.* 244, 166–177. <https://doi.org/10.1016/j.jmatprotec.2017.01.001>.
- [18] Filice, L., Ambrogio, G., Micari, F., 2006. On-line control of single point incremental forming operations through punch force monitoring. *CIRP Ann. -Manuf. Technol.* 55, 245–248. [https://doi.org/10.1016/S0007-8506\(07\)60408-9](https://doi.org/10.1016/S0007-8506(07)60408-9).
- [19] Durante, M., Formisano, A., Langella, A., 2010. Comparison between analytical and experimental roughness values of components created by incremental forming. *J. Mater. Process. Technol.* 210, 1934–1941. <https://doi.org/10.1016/j.jmatprotec.2010.07.006>.
- [20] Hamilton, K., Jeswiet, J., 2010. Single point incremental forming at high feed rates and rotational speeds: surface and structural consequences. *CIRP Ann. -Manuf. Technol.* 59, 311–314. <https://doi.org/10.1016/j.cirp.2010.03.016>.
- [21] Park, J.G., Kim, J.H., Park, N.W., Kim, Y.S., 2009. Study of forming limit for rotational incremental sheet forming of magnesium alloy sheet. *Mater. Trans.* A 41, 97–105. <https://doi.org/10.1007/s11661-009-0043-7>.
- [22] Cheng, Z., Li, Y., Li, J., Li, F., Meehan, P.A., 2022. Ultrasonic assisted incremental sheet forming: constitutive modeling and deformation analysis. *J. Mater. Process. Technol.* 299, 117365. <https://doi.org/10.1016/j.jmatprotec.2021.117365>.
- [23] Long, Y., Li, Y., Sun, J., Ille, I., Li, J., Twiefel, J., 2018. Effects of process parameters on force reduction and temperature variation during ultrasonic assisted incremental sheet forming process. *Int. J. Adv. Manuf. Technol.* 97, 13–24. <https://doi.org/10.1007/s00170-018-1886-0>.
- [24] Bai, L., Li, Y., Yang, M., Lin, Y., Yuan, Q., Zhao, R., 2019. Modeling and analysis of single point incremental forming force with static pressure support and ultrasonic vibration. *Materials* 12, 1899. <https://doi.org/10.3390/ma12121899>.
- [25] Amini, S., Hosseinpour, G.A., Pakinat, H., 2016. An investigation of conventional and ultrasonic-assisted incremental forming of annealed AA1050 sheet. *Int. J. Adv. Manuf. Tech.* 90, 1569–1578. <https://doi.org/10.1007/s00170-016-9458-7>.
- [26] Li, Y., Chen, X., Sun, J., Li, J., Zhao, G., 2017. Effects of ultrasonic vibration on deformation mechanism of incremental point-forming process. *Procedia Eng.* 207, 777–782. <https://doi.org/10.1016/j.proeng.2017.10.828>.
- [27] Lu, B., Li, Z., Long, H., Chen, F., Chen, J., Ou, H., 2017. Microstructure refinement by tool rotation-induced vibration in incremental sheet forming. *Procedia Eng.* 207, 795–800. <https://doi.org/10.1016/j.proeng.2017.10.831>.
- [28] Long, H., Peng, W.X., Chang, Z.D., Zhu, H., Jiang, Y.J., Li, Z.H., 2024. New Rosette tools for developing rotational vibration-assisted incremental sheet forming. *J. Mater. Process. Technol.* 326, 118311. <https://doi.org/10.1016/j.jmatprotec.2024.118311>.
- [29] Xu, D., Wu, W., Malhotra, R., Chen, J., Lu, B., Cao, J., 2013. Mechanism investigation for the influence of tool rotation and laser surface texturing (LST) on formability in single point incremental forming. *Int. J. Mach. Tool. Manuf.* 73, 37–46. <https://doi.org/10.1016/j.jmachtools.2013.06.007>.
- [30] Chang, Z., Li, M., Chen, J., 2019. Analytical modeling and experimental validation of the forming force in several typical incremental sheet forming processes. *Int. J. Mach. Tool. Man.* 140, 62–76. <https://doi.org/10.1016/j.jmachtools.2019.03.003>.
- [31] Gutowski, P., Leus, M., 2012. The effect of longitudinal tangential vibrations on friction and driving forces in sliding motion. *Tribol. Int.* 55, 108–118. <https://doi.org/10.1016/j.triboint.2012.05.023>.
- [32] Gutowski, P., Leus, M., 2015. Computational model for friction force estimation in sliding motion at transverse tangential vibrations of elastic contact support. *Tribol. Int.* 90, 455–462. <https://doi.org/10.1016/j.triboint.2015.04.044>.
- [33] Wu, L., Zhao, C., Cao, M., Han, X., 2021. Effect of ultrasonic and low frequency vibrations on friction coefficient at die radius in deep drawing process. *J. Manuf. Process.* 71, 56–69. <https://doi.org/10.1016/j.jmapro.2021.09.008>.

- [34] Dupont, P., Hayward, V., Armstrong, B., Altpeter, F., 2002. Single state elasto-plastic friction models. *IEEE T. Autom. Contr.* 47, 787–792. <https://doi.org/10.1109/TAC.2002.1000274>.
- [35] Chang, Z., Chen, J., 2019. Analytical model and experimental validation of surface roughness for incremental sheet metal forming parts. *Int. J. Mach. Tool. Manuf.* 146, 103453. <https://doi.org/10.1016/j.ijmachtools.2019.103453>.
- [36] Fujiyama, K., Mori, K., Matsunaga, T., Kimachi, H., Saito, T., Hino, T., Ishii, R., 2009. Creep-damage assessment of high chromium heat resistant steels and weldments. *Mater. Sci. Eng. A* 510–511, 195–201. <https://doi.org/10.1016/j.msea.2008.08.045>.
- [37] Calcagnotto, M., Ponge, D., Demir, E., Raabe, D., 2010. Orientation gradients and geometrically necessary dislocations in ultrafine grained dual-phase steels studied by 2D and 3D EBSD. *Mater. Sci. Eng. A* 527, 2738–2746. <https://doi.org/10.1016/j.msea.2010.01.004>.
- [38] Reid, J.V., Schey, J.A., 1987. The effect of surface hardness on friction. *Wear* 118, 113–125. [https://doi.org/10.1016/0043-1648\(87\)90008-1](https://doi.org/10.1016/0043-1648(87)90008-1).
- [39] Da Silva, L.R.R., Ruzzi, R.S., Teles, V.C., Sales, W.F., Guesser, W.L., Machado, A.R., 2019. Analysis of the coefficient of friction at the workpiece-tool interface in milling of high strength compacted graphite cast irons. *Wear* 426, 1646–1657. <https://doi.org/10.1016/j.wear.2019.01.111>.
- [40] Wang, X., Qi, Z., Chen, W., Xiao, Y., 2021. Study on the effects of transverse ultrasonic vibration on deformation mechanism and mechanical properties of riveted lap joints. *Ultrasonics* 116, 106452. <https://doi.org/10.1016/j.ultras.2021.106452>.
- [41] Aerens, R., Eyckens, P., Bael, A.V., Duflou, J.R., 2010. Force prediction for single point incremental forming deduced from experimental and FEM observations. *Int. J. Adv. Manuf. Tech.* 46, 969–982. <https://doi.org/10.1007/s00170-009-2160-2>.
- [42] Eyckens, P., Belkassam, B., Henrard, C., Gu, J., Sol, H., Habraken, A.M., Duflou, J. R., Bael, A.V., Houtte, P.V., 2011. Strain evolution in the single point incremental forming process: digital image correlation measurement and finite element prediction. *Int. J. Mater. Form.* 4, 55–71. <https://doi.org/10.1007/s12289-010-0995-6>.
- [43] Kaltenbrunner, T., Krückl, H.P., Schnalzger, G., Klünsner, T., Tepperneegg, T., Czettel, C., Ecker, W., 2022. Differences in evolution of temperature, plastic deformation and wear in milling tools when up-milling and down-milling Ti6Al4V. *J. Manuf. Process.* 77, 75–86. <https://doi.org/10.1016/j.jmapro.2022.03.010>.
- [44] Chang, Z., Chen, J., 2020. Mechanism of the twisting in incremental sheet forming process. *J. Mater. Process. Technol.* 276, 116396. <https://doi.org/10.1016/j.jmatprotec.2019.116396>.